Available online at www.sciencedirect.com
ScienceDirect
Organic Electronics 7 (2006) 592–599
Organic Electronics
www.elsevier.com/locate/orgel

Thin-film field-effect transistors: The effects of traps on the bias and temperature dependence of field-effect mobility, including the Meyer–Neldel rule

P. Stallinga *, H.L. Gomes

Universidade do Algarve, Facudade de Ciencias e Tecnologia, Campus de Gambelas, 8005-139 Faro, Portugal

Received 16 May 2006; received in revised form 29 September 2006; accepted 4 October 2006

Abstract

Based on the model of thin-film transistors in which the active layer is treated as two-dimensional, the effects of traps are studied. It is shown that when abundant discrete trap states are present, the field-effect mobility becomes temperature dependent. In case the traps are distributed exponentially in energy, a Meyer–Neldel rule for the temperature dependence of mobility and current results. When also the mobile states are distributed in energy, in the so-called band-tail states, the mobility is no longer thermally activated.
© 2006 Elsevier B.V. All rights reserved.

PACS: 85.30.De; 85.30.Tv

Keywords: Thin-film transistors; Traps; Meyer–Neldel rule; Temperature dependence

1. Introduction

Organic materials for electronic components are beginning to find commercial applications in consumer electronics where they serve as low cost alternatives for traditional materials. The description of the electronic behavior is still under debate while the products are already for sale. However, for increased control over the behavior, it is important to determine what are causing the properties and limitations of the final devices. An important organic electronic device is the thin-film field effect transistor (TFT), used in, for instance, switching elements in active matrix displays. Note that recently it has been shown that organic TFTs, because of the improved quality and accompanying ambipolar character of conduction, can also be the light emitting element [1,2]. Traditionally, these devices have been described by the metal-oxide-semiconductor field-effect-transistor (MOS-FET) model [3], including those devices made of organic materials [4], since this type of device is well established and described and the behavior at first glance is very similar to that of TFTs. There are however some features that are difficult to explain in the MOS-FET framework. One of the things that

* Corresponding author. Tel.: +351 969541198; fax: +351 289800030.
E-mail address: pjotr@ualg.pt (P. Stallinga).

1566-1199/$ - see front matter © 2006 Elsevier B.V. All rights reserved.
doi:10.1016/j.orgel.2006.10.003

deserve extra attention is the temperature dependence. Currents and charge-carrier mobilities of MOS-FET devices based on silicon are basically independent of temperature. On the other hand, TFTs based on organic materials do normally not show this characteristic; complicated temperature dependencies are often observed and reported.

Probably, the most remarkable feature of TFTs is the fact that, normally, the active layer is non-compatible with the substrate in terms of crystallographic properties. Often, the thin active layer has a different lattice parameter compared to the underlying insulating material (see Fig. 1 for a cross-section of a TFT). Take as an example a TFT made of silicon grown on top of silicon oxide. Especially the first mono-layers of silicon are impossible to grow with a well-defined crystallographic structure. Inevitably, many defects are created. In fact, the silicon becomes amorphous. Generally speaking, since the material of the active layer has a lattice mismatch compared to the insulating layer, defects are unavoidable. These defects can be electrically active and can, for instance, trap free charges that would otherwise contribute to external currents. Thus, these traps, normally distributed over the entire bandgap of the semiconductor, can cause severe modifications of the electronic properties of the device. In the current work, we will show how traps

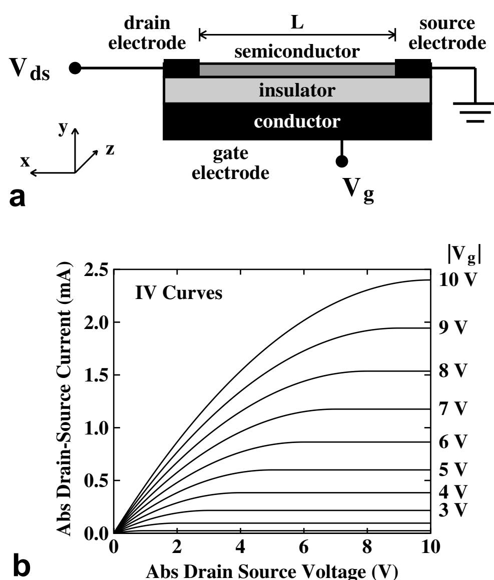

Fig. 1. (a) Cross-section of a TFT device with the names of parameters and variables used in the current work. (b) Representations of Eq. (3) with parameters as in Table 1 and $L = 10$ μm and $W = 1$ cm.

change the temperature dependence of the parameters of TFTs. Moreover, as we will show, the temperature dependence can shed light on the density of states involved in electronic conduction.

One special case of temperature dependence is the Meyer–Neldel Rule (MNR) [5]. The MNR is an observation which states that the magnitude of a process is dependent on a certain parameter, but that the dependence disappears at the iso-kinetic temperature. This behavior is truly cross-disciplinary as it is found back in many processes in nature, such as diffusion and conduction. Although not limited to the process of electronic conduction, we focus here on this field. As an example there is the observation of the MNR for ionic conductivity [6], glassy [7], poly-crystalline [8] and organic [9] materials. We will show that the current and carrier-mobility of TFTs depend on the bias conditions in a way following the Meyer–Neldel Rule when the material has abundant traps that are distributed in energy. This finding may be relevant in understanding such observations reported in electronic devices (organic and inorganic alike [10,11]). The Meyer–Neldel Rule applied to the process of electronic conduction in TFTs can best be described by the following two points: (i) The activation energy of drain–source current, I_{ds}, or as-measured carrier mobility, μ_{FET}, depends on the gate bias. (ii) There exists a temperature, known as the iso-kinetic temperature T_{MN}, where the dependence of current or mobility on bias disappears. In other words, when presented in an Arrhenius plot (logarithm of the measured quantity vs. reciprocal temperature), the curves of current or mobility are straight lines that pass through or converge to a common point. For amorphous silicon transistors, based on the model of Shur and Hack [13], we determined the immediate consequence of the presence of abundant trap states to the observation of the MNR [15]. In the current work, we show how the two-dimensional model for TFTs results in similar results. However, the results are not identical to the ones obtained with the MOS-FET model. The results and the differences will be discussed.

2. Results and discussion

Where a MOS-FET is basically a three-dimensional device, *i.e.*, has finite thickness, a TFT is best described by a in a two-dimensional way. Apart from this, it is convention to use the *inversion*-channel model to analyze the TFTs, whereas most organic TFTs are operating in *accumulation* mode.

When these two things are taken into account, a direct result is that there are no band bendings in the active layer. In other words, all voltage drop is absorbed by the insulator. The local density of charge in the active layer is directly proportional to the voltage drop across the insulator

$$\rho(x) = C_{ox}[V(x) - V_g]. \quad (1)$$

This charge can be either free holes p (for the current work we consider a p-type accumulation channel TFT), or trapped charge N_T^+. At any given point in the device, the current is proportional to the local free charge density, the free-charge (band) mobility μ_0 and the local electric field, $dV(x)/dx$:

$$I_x(x) = qWp(x)\mu_0 \frac{dV}{dx}, \quad (2)$$

with q the elementary charge, and W the channel width (the current density has been integrated over the width of the channel to get the total current passing a line at position x). In the absence of any current sources or sinks, the current $I_x(x)$ has to be constant over the entire channel length ($0 \leqslant x \leqslant L$) and equal to the externally observable current I_{ds} (see Fig. 1a for a cross-section of a device). In the absence of any traps the charge is only free charge, $\rho = p$, and it can easily be shown that in this case [14]

$$I_{ds} = -\frac{W}{L} C_{ox}\mu_0 \left(V_g V_{ds} - \frac{1}{2} V_{ds}^2 \right). \quad (3)$$

(See Fig. 1b for the IV curves). This result is very similar to the current–voltage equations of MOS-FETs [3]. For small drain–source biases, the quadratic term V_{ds} disappears from the above equation and this is then called the linear regime.

Conventionally, for MOS-FETs, the field-effect mobility μ_{FET} is defined via the derivative of the transfer curve (I_{ds} vs. V_g) in the linear regime:

$$\mu_{FET} \equiv -\frac{L}{W} \frac{1}{C_{ox} V_{ds}} \frac{\partial I_{ds}}{\partial V_g}. \quad (4)$$

Equally standard is applying this definition of μ_{FET} to TFTs, which then sometimes becomes bias or temperature dependent. Furthermore, it can be stated that at low drain–source bias, in the so-called linear regime, the charge density and electric field can be considered homogeneous along the channel. In this case, the current is proportional to the free charge density, holes (p) in the case of p-channel FETs. The mobility in the linear regime is thus proportional to the derivative of the function of the hole-density as a function of gate bias:

$$\mu_{FET} = -\frac{q\mu_0}{C_{ox}} \frac{\partial p(V_g)}{\partial V_g}. \quad (5)$$

For intrinsic TFTs this relation is linear. The as-measured mobility is therefore bias independent. (For this analysis we consider the intrinsic (band) mobility μ_0 to be temperature independent; effects of optical-phonon scattering, etc., are not included. In any case, these are slowly varying functions of temperature, such as $T^{1/2}$ [3]). The function becomes non-linear and the transfer curves with it, when – and only then – the material is full of traps. As a first attempt we try a discreet trap. In this case, the mobility is lowered significantly by the reduced ratio of free-to-total charge, and becomes temperature dependent, but remains independent of bias. This result is similar to the model of Poole and Frenkel [3] and the reasoning is as follows: Free holes (p) in the conduction band, originally induced by the gate bias, can be captured by the traps, turning these positively charged. At thermal equilibrium, the ratio of densities of holes and charged traps N_T^+ is determined by the energetic distance $E_T - E_V$ between them, the relative abundance of the levels, N_V and N_T, respectively, and the temperature T (*Note*: since the active layer is treated as purely two-dimensional, all densities have units "per square meter"):

$$\frac{p}{N_T^+} = \frac{N_V}{N_T} \exp\left(\frac{E_V - E_T}{kT}\right), \quad (6)$$

where the Boltzmann statistics function was used presupposing that the Fermi level is far away from both the conductive as well as the trap state levels (for the simulations, however, the full Fermi–Dirac distribution was used). The total charge induced in the channel is proportional to the gate bias (Eq. (1)):

$$p + N_T^+ - n = -C_{ox} V_g / q. \quad (7)$$

The current is only proportional to the free hole density because the trapped states, by definition, do not contribute to current and the density of electrons is insignificant. The solution of the above equations is that the current is linearly proportional to the gate bias and that the effective, as-measured mobility of Eqs. (4) and (5), defined via the derivative of the transfer curve, is therefore depending on temperature, but not on bias

$$\mu_{FET} \approx \mu_0 \frac{N_V}{N_T} \exp\left(-\frac{E_T - E_V}{kT}\right). \quad (8)$$

In other words, the Arrhenius plots of mobility are straight lines; independent of bias, the slope of the

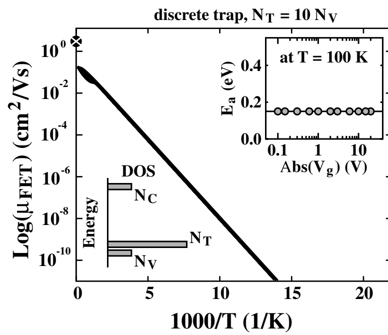

Fig. 2. Arrhenius plot of mobility for the case of an abundant discrete trap. In this particular case, $N_T = 10N_V$. The mobility is strongly temperature dependent and the plot reveals the trap depth of 150 meV, independent of bias. The insets show the schematic DOS and the activation energy of mobility (and current) as a function of gate bias. The symbol ⊗ at the mobility axis indicates the free-hole mobility μ_0.

plot reveals the activation energy of mobility, which is then equal to the depth of the trap level, $E_a = E_T - E_V$, see Fig. 2. This result is similar to the Poole–Frenkel model [3], or the variable-range hopping model of Horowitz [4]. Note that extrapolation of the curves to $T = \infty$ gives an effective prefactor in the mobility equal to $\mu_\infty = \mu_0 N_V/N_T$, which can be well below the free-hole band value μ_0 when the traps are abundant. For the figure, $N_T = 10N_V$ was used.

The assumption was made here that the trap states are truly abundant, effectively unlimited: $N_T \gg N_V$. When this is not the case, the trap states can be exhausted and, once all filled, the induced charge is necessarily free charge (holes) and the mobility returns to the band value μ_0. In the above calculations, it involves replacing the Boltzmann distribution approximation by the full Fermi-Dirac distribution function. The traps become depleted when the induced charge density is comparable to the trap density. This defines the trap-free-limit voltage for the gate bias

$$V_{tfl} = -qN_T/C_{ox}. \tag{9}$$

In Fig. 3, a transition case is shown with the trap density equal to the effective density of valence band states, $N_T = N_V$. For this specific case, $V_{tfl} = -10.4$ V. For gate biases below this voltage, the activation energy is equal to the trap depth (150 meV), while above it, the mobility rapidly becomes independent of temperature and settles at the free-hole value μ_0, as can be seen in the figure. In this case, it is not easy to give an algebraic solution. Fig. 3b shows the bias dependence of the mobility for different temperatures, which is based on numerical simulations: For a certain bias V_g, the Fermi level that zeros the total charge minus induced charge is found by a numerical algorithm as described by Ref. [12]. Once the Fermi level is found, the free charge is determined by substituting this energy in the free hole distribution $p(E_F)$. The voltage is stepped by a tiny amount and the free charge is calculated again. The mobility is then the derivative according to Eq. (5). (*Remark*: this technique was also used for Fig. 2). As can be seen, for $-V_g > -V_{tfl}$ the mobility is equal to the free-hole value indicated by ⊗ at the mobility axis. In fact, Eq. (9) gives a fast way of determining the trap density, provided the rapid transition in the transfer curves is observed that allows for a determination of V_{tfl}.

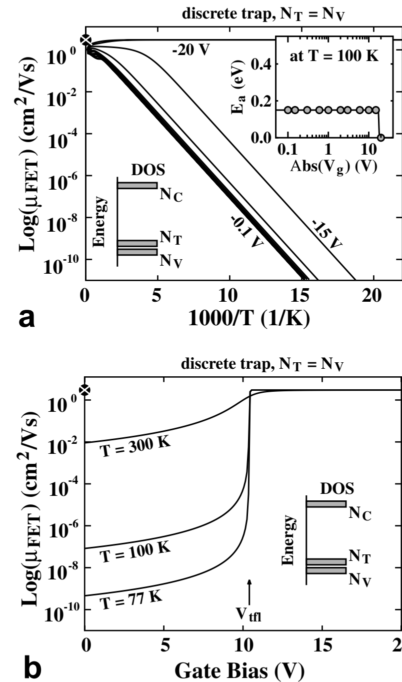

Fig. 3. (a) Arrhenius plot of mobility for a discrete trap with density equal to the effective density of valence band states, $N_T = N_V$. The activation energy is equal to the trap depth for biases below the trap-free-limit voltages $V_g < V_{tfl}$. For larger biases, the mobility is no longer thermally activated and the plots resemble those of trap-free devices. The insets show the schematic DOS and the activation energy of mobility (and current). The symbol ⊗ at the mobility axis indicates the free-hole mobility μ_0. (b) The bias dependence of mobility at three different temperatures. The trap-free limit voltage, V_{tfl} of Eq. (9) is indicated.

Inspired by the model of Shur and Hack [13] we then tried a model in which the trap states are distributed in energy. This, as we determined, can give rise to a bias- and temperature-dependent mobility.

Using a normal valence band and trap states N_T exponentially distributed in energy,

$$N_T(E) = g_{T0} \exp\left(\frac{E_V - E}{kT_2}\right) \tag{10}$$

with E the energy of an electron, g_{T0} the density of states (DOS) of traps at the valence band E_V, k Boltzmann's constant, and T_2 a parameter describing the distribution (the slope of a logarithmic plot of the DOS, see Fig. 4). When following the same reasoning as followed for the discrete trap, but with a convolution over trap states in Eqs. (6) and (7), it can be shown that the drain–source current is (see Appendix)

$$I_{ds} = q\mu_0 \frac{W}{L} V_{ds} N_V \left(\frac{-C_{ox}V_g}{qN_{T0}(T)}\right)^{T_2/T} \tag{11}$$

with

$$N_{T0}(T) = \alpha(T) g_{T0} \frac{k^2 T_2^2}{kT_2 - kT} \tag{12}$$

with $\alpha(T)$ a slowly varying function of temperature (and therefore irrelevant for the discussion), oscillating between 1 and 0.8 in the temperature range 0–T_2, with a minimum halfway. The as-measured mobility is proportional to the gate-bias derivative of this function (see Eq. (4)):

$$\mu_{FET} = \frac{T_2}{T} \mu_0 \frac{N_V}{N_{T0}(T)} \left(\frac{-C_{ox}V_g}{qN_{T0}(T)}\right)^{T_2/T-1}. \tag{13}$$

It is immediately clear that (i) the mobility depends on gate bias and (ii) the dependence disappears at a temperature $T = T_2$, thus following the Meyer–Neldel Rule, with $T_{MN} = T_2$. Fig. 5 shows simulations of the above equation with parameters as in Table 1. From this figure it can be seen that, because of the effects of the factor T in the denominator of the above equation, as well as the temperature dependence of α, the iso-kinetic temperature falls slightly below T_2 and the curves do not exactly extrapolate to a single point. However, in most cases will the instrumental resolution be too low to accurately determine this small deviation. Note also the sharp drop in current when the temperature approaches T_2. This is due to the factor $1/(kT_2 - kT)$ in Eq. (12), which diverges for $T \to T_2$. To our knowledge, no reports in literature exist for measurements at or in the vicinity of the iso-kinetic temperature; in all cases, T_{MN} is found by extrapolation.

Analyzing Eqs. (11) and (13) it is easily shown that the activation energy of the field mobility (and current alike), as measured via the slope of an Arrhenius plot, depends on the bias in the following way

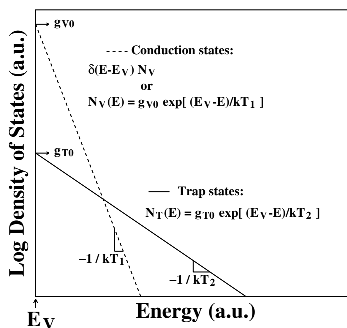

Fig. 4. Density of states used for the last calculations (Figs. 5 and 6). The trap states (solid line) are exponentially distributed in energy. For the conduction states, two distributions are tried: A discreet band at $E = E_V$ and an exponentially decaying function (dashed line). The former results in the observation of the MNR with bias and temperature dependent current and mobility, see Fig. 5. For the latter, only the bias dependence remains and the temperature dependence nearly vanishes, see Fig. 6.

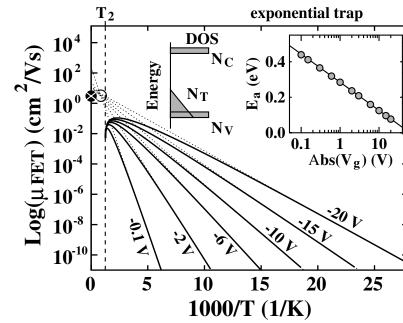

Fig. 5. Graphical representation of temperature-dependent as-measured mobility of Eq. (13) of a system with a DOS as in Fig. 4, namely an exponential distribution of trap states and discrete conduction states. Parameters as in Table 1, with gate biases from −0.1 V to −20 V as indicated. The open circle (○) represents the Meyer–Neldel point (T_{MN}, μ_{MN}). The inset shows the effective activation energy as a function of bias.

Table 1
Parameters used to generate figures

Parameter	Value	Unit
N_V	1.04×10^{16}	m^{-2}
N_T	1.04×10^{17}	m^{-2}
C_{ox}	160	$\mu F/m^2$
g_{T0}	10^{18}	$m^{-2}\,eV^{-1}$
g_{V0}	10^{17}	$m^{-2}\,eV^{-1}$
T_2	800	K
T_1	300	K
μ_0	3	$cm^2\,V^{-1}\,s^{-1}$

$$E_a \equiv -\frac{d\ln(\mu_{FET})}{d(1/kT)} = kT_2\ln(N_{T0}) - kT_2\ln(-C_{ox}V_g/q). \quad (14)$$

This is shown in the inset of Fig. 5. Thus, the activation energy of mobility or current does not reveal the depth of an energetic level. Rather, it depends on the parameters of the distribution (T_2 and g_{T0}) and the bias.

At this moment it is interesting to point out the difference between our model and the model of Shur and Hack [13]. Where they have a factor of $2T_2/T-1$ in the exponent in the current, we have T_2/T (Eq. (11)). This results, in our case, in an infinite iso-kinetic temperature for the current, whereas they have $T_{MN} = 2T_2$ [15]. For mobility, both models arrive at $T_{MN} = T_2$; the dependence of mobility on bias disappears at this temperature, as shown by Eq. (13).

A more fundamental difference is that Shur and Hack use exponential distribution for both the traps states as well as the valence band states (the so-called "tail states"), where we use only a distributed trap state, while we maintain a Dirac-delta function for the DOS of the valence band. When we include exponentially distributed tail states,

$$N_V(E) = g_{V0}\exp\left(\frac{E_V - E}{kT_1}\right), \quad (15)$$

with similar reasoning we arrive at a strongly bias dependent, but temperature independent mobility (see Appendix),

$$\mu_{FET} = \frac{T_2}{T_1}\mu_0\frac{N_{V0}(T)}{N_{T0}(T)}\left(\frac{-C_{ox}V_g}{qN_{T0}(T)}\right)^{T_2/T_1-1} \quad (16)$$

with

$$N_{V0}(T) = \beta(T)g_{V0}\frac{k^2T_1^2}{kT_1 - kT} \quad (17)$$

with T_1 the parameter describing the distribution of band-tail states, see Fig. 4, and β a function equal to α but scaled with T_1 instead of T_2. Fig. 6 shows a simulation of the mobility as a function of temperature and bias. Interesting in this respect is the observation by us of exactly such a behavior [16], something that is inexplicable in the theory of Shur and Hack.

Fig. 7 compares the various models described in this work and the model of Shur and Hack [13]. For the latter we used a value of 0.484 eV for their parameter E_{F0} and the value for their parameter g_{F0} (defining the density of states at E_{F0}) can then be found by extrapolating our g_{T0} to $E = E_{F0}$ in Eq. (10) and dividing it by 1 nm. This gives $g_{F0} = 8.93 \times 10^{23}/m^3$ eV. As can be seen, the model of Shur and Hack with conduction and donor states

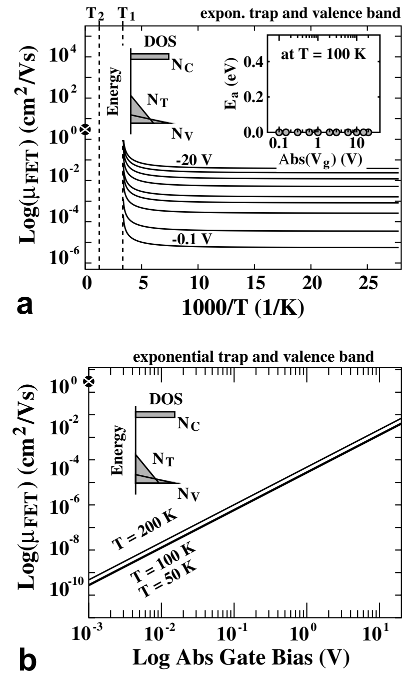

Fig. 6. Graphical representation of temperature-dependent as-measured mobility of Eq. (16) of (a) system with a DOS as in Fig. 4, namely an exponential distribution for both the trap states as well as the conduction states. Parameters as in Table 1, with gate biases from −0.1 V to −20 V as indicated. The mobility is strongly bias dependent, but independent of temperature; the inset shows the effective activation energy as a function of bias. (b) Shows the bias dependence of mobility for three different temperatures, which clearly follow a power law.

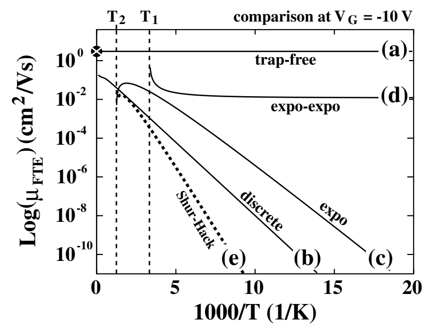

Fig. 7. Comparison of the various models: (a) trap-free model, (b) abundant discrete trap, (c) exponentially distributed trap, (d) exponentially distributed trap and conduction band, (e) model of Shur and Hack (with $E_{F0} = 0.484$ eV, $g_{F0} = 8.93 \times 10^{23}/m^3$ eV, $N_V = 1.04 \times 10^{25}/m^3$, $\varepsilon = 11.9\varepsilon_0$ and other parameters as in Table 1).

exponentially distributed in energy behaves much like our model with only the trap states distributed exponentially in energy. Noteworthy, the model of Shur and Hack was developed for amorphous silicon devices based on the MOS-FET model with a three-dimensional active layer, while our model is based on the two-dimensional accumulation-channel TFT model.

In conclusion, we have shown that a material that is full of traps (electronic states that can capture the free charge), when used in the active layer of TFTs, results in a strongly temperature dependent current and mobility. When the trap states are distributed in energy the mobility also becomes bias dependent, resulting in the observation of the so-called Meyer–Neldel Rule. The iso-kinetic temperature, the temperature where the as-measured mobility is independent of bias, is equal to T_2, the parameter describing the DOS of the traps. When also the conduction states are distributed in energy, the mobility loses its temperature dependence. As such, a set of Arrhenius plots for different biases may serve as a rapid evaluation tool of the quality of the material. More specifically, they give direct insight into the density-of-states governing the conduction. In cases, where a sharp transition in mobility is observed in the transfer curves the density of (discrete) traps can directly be determined via the trap-free-limit voltage V_{tfl}, see Eq. (9) and Fig. 3b.

As a final remark, it has to be pointed out that in this analysis at all times thermal equilibrium is assumed. Especially, for deep traps this equilibrium can take very long time to establish, in which case the electrical characteristics will depend on things such as the scanning speed and even the history of the device in case of extremely deep electronic levels.

Acknowledgements

This work was financed by the Portuguese Foundation for Science and Technology (FCT), Project POCTI/FAT/47956/2002 and the Programa Operacional Sociedade do Conhecimento, Research Unit No. 631, CEOT.

Appendix. Derivation of Eqs. (11) and (16)

To arrive at Eq. (11) a density of states (DOS) exponentially decaying in energy is used,

$$N_{\text{T}}(E) = g_{\text{T0}} \exp\left(\frac{E_{\text{V}} - E}{kT_2}\right) \tag{18}$$

with g_{T0} the density of states at $E = E_{\text{V}}$ and T_2 the decay rate, parameters that describe the distribution. The dependence of N_{T}^+ on the position of the Fermi level thus becomes

$$N_{\text{T}}^+(E_{\text{F}}) = \int_{-\infty}^{\infty} N_{\text{T}}(E)[1 - f(E - E_{\text{F}})]\,\text{d}E \tag{19}$$

with f the Fermi–Dirac distribution function,

$$f(E - E_{\text{F}}) = \frac{1}{1 + \exp[(E - E_{\text{F}})/kT]}. \tag{20}$$

The integral of Eq. (19) converges when $T < T_2$. To a good approximation, the solution can be found by dividing the integral into two parts, see Fig. 8. In the first part, below E_{F}, the slope is $1/kT - 1/kT_2$ as a result of the difference of slopes in N_{T} and the exponential approximation for $1 - f$. Above E_{F}, $1 - f$ is considered unity and the resulting slope is $1/kT_2$. With this help, it can easily be shown that the integral is equal to

$$N_{\text{T}}^+(E_{\text{F}}) = N_{\text{T0}}(T) \exp\left(\frac{E_{\text{V}} - E_{\text{F}}}{kT_2}\right), \tag{21}$$

where N_{T0} is as in Eq. (12) in which $\alpha(T)$ an ad hoc correction factor that compensates for the error of integration; compare the rounded distribution of N_{T}^+ of Fig. 8 and the triangular integration described above. Numerical simulations show that $\alpha(T)$ oscillates between 1 and 0.8 in the temperature range 0–T_2 (see Fig. 9). This makes N_{T0} essentially temperature independent for T not very close to T_2. For $T \geqslant T_2$ the integral diverges.

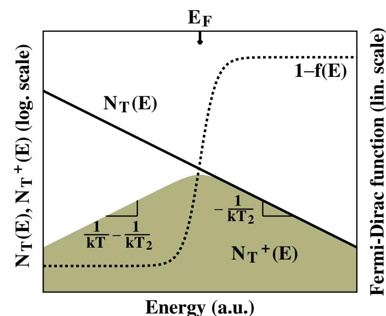

Fig. 8. Graphical schematic of the distribution in energy of trap states $N_T(E)$ (solid line) and charged trap states N_{T}^+ (shaded area). The latter is a result of a multiplication of the former by the Fermi–Dirac function $1 - f(E)$ (dashed line). This shows that the total trapped charge N_{T}^+ as a function of Fermi level, see the integral of Eq. (21), can easily be approximated by dividing the integral into two parts.

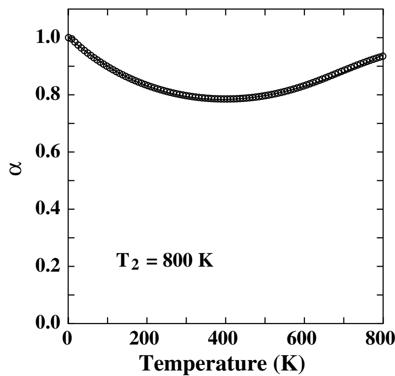

Fig. 9. The ad hoc correction factor α as a function of temperature, calculated numerically. α is a slowly varying function of T and its contribution to the calculation is minimal. For the calculations, α is approximated by a third-order polynomial (solid line).

If the conduction states are assumed to be discrete in energy, a standard valence band with N_{V} states at E_{V}, the density of holes follows

$$p = N_{\mathrm{V}} \exp\left(-\frac{E_{\mathrm{F}} - E_{\mathrm{V}}}{kT}\right). \tag{22}$$

These two densities of p and N_{T}^{+} can be introduced into the induced charge equation (Eq. (7)), ignoring the tiny contribution of the free electron density n

$$p + p^{T/T_2}\left(\frac{N_{\mathrm{T0}}(T)}{N_{\mathrm{V}}^{T/T_2}}\right) = \frac{-C_{\mathrm{ox}}V_{\mathrm{g}}}{q}. \tag{23}$$

For high densities of traps, the first term is negligible and the free hole density can then easily be determined as

$$p(V_{\mathrm{g}}) = N_{\mathrm{V}}\left(\frac{-C_{\mathrm{ox}}V_{\mathrm{g}}}{qN_{\mathrm{T0}}(T)}\right)^{T_2/T}. \tag{24}$$

The current can then be found by Eq. (2), where in the linear regime, p is homogeneous in space and $\mathrm{d}V/\mathrm{d}x = V_{\mathrm{ds}}/L$. This results in Eq. (11).

Next, conduction states exponentially distributed in energy are tried

$$N_{\mathrm{V}}(E) = g_{\mathrm{V0}} \exp\left(\frac{E_{\mathrm{V}} - E}{kT_1}\right) \tag{25}$$

with g_{V0} the density-of-states at $E = E_{\mathrm{V}}$, and T_1 a parameter describing the distribution (see Fig. 4). Similar integration techniques result in

$$p(E_{\mathrm{F}}) = N_{\mathrm{V0}}(T) \exp\left(\frac{E_{\mathrm{V}} - E_{\mathrm{F}}}{kT_1}\right) \tag{26}$$

with N_{V0} as in Eq. (17), in which β is a function similar to α, but scaled with T_1 instead of T_2. Again, this can be substituted in the induced-charge equation (Eq. (7)) and for high trap densities, the free charge density follows

$$p(V_{\mathrm{g}}) = N_{\mathrm{V0}}(T)\left(\frac{-C_{\mathrm{ox}}V_{\mathrm{g}}}{qN_{\mathrm{T0}}(T)}\right)^{T_2/T_1} \tag{27}$$

substitution into Eq. (2) and using the field-mobility definition of Eq. (4) yields Eq. (16).

References

[1] C. Santato, R. Capelli, M.A. Loi, M. Murgia, F. Cicoira, V.A.L. Roy, P. Stallinga, R. Zamboni, S.F. Karg, M. Muccini, Synth. Met. 146 (2004) 329.
[2] S. Setayesh, D. de Leeuw, M. Büchel, T. Anthopoulos, E. Smits, P. Blom, in: Proceedings of the ECME 8 Abstract book, 2005, p. 15.
[3] S.M. Sze, Physics of semiconductor devices, second ed., Wiley Interscience, 1981.
[4] G. Horowitz, Adv. Mater. 10 (1998) 365.
[5] W. Meyer, H. Neldel, Z. Tech. 18 (1937) 588.
[6] K.L. Ngai, Solid State Ionics 105 (1998) 231.
[7] K. Shimakawa, F. Abdel-Wahab, Appl. Phys. Lett. 70 (1997) 652.
[8] S.K. Ram, S. Kumar, R. Vanderhaghen, P. Roca i Cabarrocas, J. Non-Crystalline Solids 299–302 (2002) 411.
[9] E.J. Meijer, M. Matters, P.T. Herwig, D.M. de Leeuw, T.M. Klapwijk, Appl. Phys. Lett. 76 (2000) 3433.
[10] Y. Lubianiker, I. Balberg, J. Non-Crystalline Solids 227–230 (1998) 180.
[11] M. Kondo, Y. Chida, A. Matsuda, J. Non-Crystalline Solids 198–200 (1996) 178.
[12] W.H. Press, S.A. Teukolsky, W.T. Vetterling, B.P. Flannery, Numerical Recipes in C, 2nd ed., Cambridge University Press, 1992. Available online at http://www.nr.com .
[13] M. Shur, M. Hack, J. Appl. Phys. 55 (1984) 3831.
[14] P. Stallinga, H.L. Gomes, Opt. Appl. 36 (2006).
[15] P. Stallinga, H.L. Gomes, Org. Electr. 6 (2005) 137.
[16] P. Stallinga, H.L. Gomes, F. Biscarini, M. Murgia, D.M. de Leeuw, J. Appl. Phys. 96 (2004) 5277.